HHS Public Access

Author manuscript

Nano Lett. Author manuscript; available in PMC 2014 November 18.

Published in final edited form as:

Nano Lett. 2013 August 14; 13(8): 3836–3842. doi:10.1021/nl401860f.

Strain-induced Large Exciton Energy Shifts in Buckled CdS Nanowires

Liaoxin Sun[1,¶], **Do Hyun Kim**[1,2], **Kyu Hwan Oh**[2], and **Ritesh Agarwal**[1,*]

[1]Department of Materials Science and Engineering, University of Pennsylvania, Philadelphia, PA 19104

[2]Department of Materials Science and Engineering, Seoul National University, Seoul 151-742, Republic of Korea

Abstract

Strain engineering can be utilized to tune the fundamental properties of semiconductor materials for applications in advanced electronic and photonic devices. Recently, the effects of large strain on the properties of nanostructures are being intensely investigated to further expand our insights into the physics and applications of such materials. In this letter, we present results on controllable buckled cadmium-sulfide (CdS) optical nanowires (NWs), which show extremely large energy bandgap tuning by >250 meV with applied strains within the elastic deformation limit. Polarization and spatially-resolved optical measurements reveal characteristics related to both compressive and tensile regimes, while micro-reflectance spectroscopy clearly demonstrate the effect of strain on the different types of excitons in CdS. Our results may enable strained NWs-based optoelectronic devices with tunable optical responses.

Keywords

nanowire; strain; CdS; photoluminescence; reflectance

Strain-engineering offers attractive prospects for understanding and tuning the properties of materials and also for the design of next generation of devices with new functionalities [1-7]. Recently, many intriguing reports on strain-dependent electronic and optical properties of nanostructures, *e.g*. carbon nanotubes and nanowires (NWs), have been published [8-18], which are greatly expanding our understanding of these nanomaterials. Due to large surface-volume ratio and high crystal quality, nanostructures can withstand large strains without fracture and hence are more useful for flexible device applications [11, 19]. More recently, opto-mechanical coupling in direct band-gap semiconductor NWs with strain has been reported with remarkable optical features including large emission energy shifts, fine exciton splitting, and size-dependent band-gap tuning [19-22]. Some of the techniques to produce strain in NWs have included using glass or probe tips [19-20] for

*Corresponding Author To whom correspondence should be addressed. riteshag@seas.upenn.edu.
¶On leave from Shanghai Institute of Technical Physics of the Chinese Academy of Sciences

Supporting Information Available. PL measurements on a highly buckled CdS NW and temperature-dependent μ-reflectance and μ-PL spectroscopy of CdS NWs on PDMS substrate. These materials are available free of charge via the internet at http://pubs.acs.org.

mechanically bending the wires and mounting the NWs on piezoelectric stages [21, 22]. These techniques, although impressive, are complex, require manipulation of one or few devices at a time and are limited to the maximum amount of stress that can be applied to the nanostructures. Elastomeric substrates have paved a new way for developing stretchable/bendable electronics, such as, paper-like displays, flexible transistors and diodes, and wearable sensors [23-26]. More interestingly, by using plastic substrates, deformed semiconductor thin-films, nanowires, and nanobelts have been obtained, which are favorable for fabricating high-performance flexible electronic devices [27-31].

Cadmium Sulfide (CdS), a semiconductor with a wurtzite structure and a direct electronic bandgap of ~2.46 eV at room temperature, has long been studied because of its potential applications in optoelectronic devices. CdS NWs or nanoribbons functioned as microcavity show remarkable optical and photonic properties such as increased light-matter coupling strengths, waveguides, photonic and plasmonic lasers, and optical switches [32-37]. In addition, the elastic modulus of CdS nanowire has been measured, which obtained values ranging from 95 GPa to 196 GPa (higher than that of bulk CdS, 62 GPa), depending on the diameter, surface and crystal quality of nanowires [38]. It would be interesting to study the effect of large strains on the optical and electronic properties of CdS NWs in order to further understand its properties under extreme conditions, which is likely to experience large strains for flexible electronics/photonics applications. Recently, by using a glass tip to manipulate the straight nanowires to a curved geometry, strain-induced redshift of cathdoluminescence peaks in CdS NW was reported [39]; however, the bandgap tuning range of CdS NW was quite small with 32 meV shift under a strain gradient of 0.7 cm^{-1}. Furthermore, since the techniques for manipulating nanowires for optical measurements was limited by the amount of strain, the effect of strain on the properties of different types of excitons (A, B and C in CdS) could not be studied.

In this letter, we present the optical properties of buckled CdS NWs, which show a large tuning of the excitons states at large strains. By using micro-photoluminescence (μ-PL) spectroscopy, the periodic modulation of energy bandgap of CdS NW is demonstrated to be as large as 250 meV at ε_{outer}= 11% tensile strain. Moreover, we find the distinct polarization responses for compressive and tensile strained areas of buckled NWs and by using micro-reflectance (μ-R) technique, we observed that the origin of distinct polarization properties mainly originate from the different strain-dependent responses of the A- and B-exciton energy shifts.

CdS NWs (grown along the c-axis) were grown via the vapor-liquid-solid method as reported elsewhere [40] and then transferred on pre-strained flexible substrates. Figure 1(a) shows schematically the procedure for obtaining in-plane buckled NWs on polydimethylsiloxane (PDMS) substrates. As-grown CdS NWs were first dry transferred from a silicon oxide substrate to a polyimide film. Subsequently, the NWs transferred on the polyimide film were carefully contacted at the center of pre-strained PDMS surface to ensure that the nanowires were subjected to uniform compressive strain. During the transfer to the PDMS substrate, the polyimide substrate was mechanically slid along the PDMS pre-strain direction to ensure that most NWs were aligned and hence buckled in-plane after the release of tensile strain (Figure 1 (b-d)). The optical properties of buckled nanowires were

measured with a home-made μ-PL and μ-R system. Unless mentioned otherwise, all μ-PL and μ-R spectra were measured with nanowires at a temperature of 77 K to obtain the exact exciton energy positions (Supplementary Information: Experiments and methods).

Fig. 2(a) shows a bright field optical image of a typical buckled CdS nanowire with an in-plane wavy geometry on a PDMS elastomeric substrate with the antinode (bent regions) positions marked by labels p1 to p9. The μ-PL spectral mapping data, consisting of more than 100 normalized spectra measured along the buckled nanowire long axis with a scanning excitation step of 0.8 μm from p1 to p9 (Fig. 2(b)) along with a corresponding waterfall plot (Fig. 2(c)) clearly shows that the exciton emission peak shifts periodically as the excitation laser moves from the node (straight regions) to the antinode positions. The regions from where the maximum redshifted spectra are obtained correspond exactly to the antinode positions labeled in Fig. 2(a), which are regions of highest strain. Furthermore, moving from p1 to p9, it can be observed that the curvature of the bent regions decreases gradually (especially from p4 – p9), which directly corresponds to the reduction in the observed spectral redshift, suggesting that the observed shifts directly correlate with the extent of strain in the nanowire.

The redshift of the exciton peak is mainly caused by the tensile strain ε_{outer} in the outer surface of curved nanowire, which can be roughly estimated by the local radius of curvature, ρ, and diameter, *D*, of nanowire ($\varepsilon_{outer} = D/2\rho$) [19,37]. With the decrease of curvature from p4 to p9, the measured exciton redshifts gradually reduced as shown in Figs. 2(b) and (d). Unlike the previously reported results observed for CdS and ZnO NWs where the observed redshift was small and limited by the techniques for straining the NWs, a huge redshift (~200 meV) of exciton emission peak is observed at the antinode part (p4, with ε_{outer}=~9%) of the wavy nanowire in our experiment. Measurements conducted on highly curved nanowires revealed redshifts as large as 250 meV (with strain ε_{outer}=~11%), and is amongst the highest ever reported for direct bandgap materials (see supporting information Fig. S-2). These results demonstrate clearly that the high quality CdS nanowires indeed possess very strong bendability. The spectral broadening at the curved part (Peak 2, Fig. 2(d)) may be attributed to the bending deformation-induced broadening of the gaps between different subbands in the conduction band [20] and also could be due to the inhomogeneous strain distribution both in the cross section and along the c-axis (growth axis) of the nanowire. Because of the large tensile strain, the redshifted Peak 2 (Fig. 2(d)) moves significantly to the low energy side of the spectrum with no overlap with Peak 1, which facilitated our study and analysis for these two peaks in the PL. It is interesting to note that as the excitation scanning laser moves from the node to the antinode position, the initial emission peak does not disappear completely but shows up as a much smaller peak (Peak 1) at the antinode (Fig. 2(d)), which can be also observed at each antinode position in the PL mapping. We also present the PL spectrum of CdS NW without any strain (Fig. 2(d) top) for reference; both A- and B-exciton peaks are clearly observed, which imply that the CdS nanowires have high optical quality [40]. Compared with the PL spectra of a buckled nanowire, we can see that the emission peak (red curve) from the node region of the buckled nanowire shows some broadening and is slightly blueshifted (Fig. 2(d)). The optical properties and the underlying mechanisms of these emission peaks will be discussed in detail later.

To demonstrate the deformation properties and controllability of strained nanowires on PDMS, we performed real-color emission imaging under different buckling curvatures at room temperature. A custom-built strain stage was used to control the curvature of the wavy nanowires, and a pair filters was place in the detection path of the microscopy set-up to help obtain emission-based images(see supporting information: experiments and methods 4 and Figure. S-1). Fig. 3(a) is a darkfield image of a typical wavy nanowire, and the corresponding real-color image is shown in Fig. 3(b), from where we can see clearly that the color of nanowire shows a periodic modulation from the nodes (blue color) to the antinode regions (green color). This behavior is consistent with the μ-PL mapping of the wavy nanowire (Fig. 2(b)), and can be understood by tensile strain-induced energy bandgap shrinking at the outer part of the antinode region. For the node regions, bandedge emission occurs at a wavelength ~500 nm (room temperature) which is quite close to the transmission raising edge of the 488 nm filters, the reflected and emitting light from the nanowire body would dominated the image of the NW, which appears blue. While for the antinode regions, the bandgap shrinking at the outer part would lead to the emission redshift to the 520 nm-540 nm range and hence enters the transmission range of the long pass 488 nm-filters, making the image of these regions appear more green. By using a strain stage, we carried out the real-color imaging measurements of the wavy nanowire while gradually changing the curvature of the bent region. As shown in Fig. 3(c), buckled nanowire on PDMS can be gradually elongated to revert back to the original straight geometry by releasing the stress, which is accompanied by the change of the green color at the antinode regions back to blue, similar to the color at the nodes. This demonstrates that the buckled parts of the NW were under elastic deformation and the deformation-caused local strain and the bandgap variation can be controlled reversibly, which is essential for the design of reconfigurable opto-mechanical-devices.

To understand the origin of the two emission peaks (Peaks 1 and 2 in Fig. 2(d)), we performed polarization dependent μ-PL measurements at the antinode region of a wavy NW (illustrated in Fig. 4(a)). The two polarization directions, σ and π, are illustrated in Fig. 4(a), *i.e*. light with electric field component (**E**) perpendicular to the c-axis of wavy nanowire is defined as σ-polarized (**E**⊥**c**-axis and **k**⊥**c**-axis), while light with electric field component (**E**) parallel to the c-axis of the wavy nanowire is defined as π-polarized (**E**//**c**-axis and **k**⊥**c**-axis). It is observed that the redshifted emission peak (Peak 2) is predominantly σ-polarized, while Peak 1 shows significant π-polarized component (Fig. 4(a)). By using the equation $\rho=\frac{I_\sigma - I_\pi}{I_\sigma + I_\pi}$ (where ρ is the polarization ratio, I is the intensity of σ- or π-polarized PL peak.), the polarization ratio of 78% for Peak 1 and 87% for Peak 2 are obtained. This unique polarization behavior implies the different origins for these two peaks.

To further study the properties of the two peaks (Peaks 1 and 2 in Fig. 2(d) and Fig. 4(a)), spatially resolved μ-PL mapping along the radial direction of the wavy nanowire was carried out (Fig. 4(b)). Although the laser spot size is ~800 nm and detector's spatial resolution ~200 nm, by carefully controlling the relative position of the wavy nanowire to the excitation laser position, we can collect the light signals from inner surface (under compressive strain) to outer surface (tensile strain) gradually. In order to get more intensity

variation of Peak 1 as the laser is scanned from the inner to the outer surface, athicker nanowire (diameter ~300 nm) is chosen for the spatially-resolved measurement. Although the signals cannot be completely resolved from the inner to the outer regions, the relative contributions can change upon scanning. It can be seen (Fig. 4(c)) that Peak 1 gradually disappears as the excitation spot moves from the inner (compressive) to the outer (tensile) surface of the wavy nanowire. These measurements confirm that Peak 1 originates from the inner part and is a consequence of compressive strain in the NW. Interestingly, Peak 2 is always present with little or no change in intensity as the excitation spot is scanned, which can be explained by the exciton diffusion process; as mentioned above, the inhomogeneous strain distribution across the cross section would cause a bandgap gradient from the inner to the outer surface; excitons excited in the compressively strained region would diffuse to the outer surface experiencing tensile strain (lower bandgap). Since the exciton diffusion length is typically ~1 μm [34], which is much greater than the typical wire diameters, it is quite likely that the excitons can diffuse from the compressively strained to the tensile strained region and recombine to generate Peak 2. Thus even if the compressively strained region were to be excited solely, the exciton PL from tensile strained part would still be observed.

In CdS, a semiconductor with wurtzite crystal structure, the conduction band is predominantly s-like state with Γ7 symmetry, whereas the valence band is p-like state, which is split into three bands due to the crystal-field effect and spin-orbit interaction. Thomas *et al*. assigned the three bands as excitons A-Γ9, B-Γ7 and C-Γ7 through reflectance and PL measurements [41]. According to the selection rules, all three excitonic transitions are allowed for σ-polarization, while in π-polarization, both the B- and C-excitons are still allowed but A-exciton is forbidden. Here it is worthy to note that in PL measurements, the C-exciton cannot be observed due to its high energy from where the carriers can rapidly relax to the lower lying exciton states (A and B), and the B-exciton shows a much stronger π-polarized emission than in comparison to σ-polarized. As previously mentioned, Peaks 1 and 2 display different linear polarizations at the antinode regions of the wavy nanowire (Fig. 3(a)). It is safe to assign the strong σ-polarized red shifted Peak 2 to A-exciton recombination, while the π-polarized Peak 1 to B-exciton (or C-exciton) recombination under compressive strain. The C exciton is typically observed at 2.619 eV at 77 K under strain-free conditions, which is much higher than B- (2.560 eV) and A-excitons (2.540 eV) [41]. In our data, Peak 1 typically appears in the 2.550 eV to 2.570 eV energy range for all measured nanowires. The observed energy uncertainty may be caused by the different adhesion force between different nanowires and PDMS substrate (which under cooling can lead to slightly different strain conditions) and also due to some temperature variation of the PDMS substrate due to its poor thermal conductivity. Regardless, the position of Peak 1 is ~50 meV lower than the value of the C-exciton in unstrained CdS and considering the fact that the compressive strain will further increase the C-exciton energy, the possibility of Peak 1 originating from C-excitons can be ruled out. Therefore, we assign Peak 1 to B-exciton recombination from the compressive strained part of the wavy nanowire.

To further verify the above assignments to the observed PL peaks, we performed μ-R measurements to study the exciton states of a single NW. Unlike PL spectroscopy, in which the linewidth broadening of emission peaks may cause the free exciton states to become

indistinguishable, the reflectance spectra can also provide more insights to determine the origin of the spectral feature. In addition, to reveal how strain affects exciton states of the NWs on the PDMS substrate, we conducted polarized μ-R and μ-PL spectral measurements on the same NW (diameter: ~150 nm) both on Si (with a 300 nm layer of SiO_2) and on PDMS substrates for direct comparison. Fig. 5(a) (top) shows the polarized reflectance spectra of a CdS nanowire on Si substrate at 77 K. Based on the selection rules, A- (2.540 eV), B- (2.560 eV) and C-exciton states (2.615 eV) can be easily assigned and are almost the same as reported in the literature [41]. The corresponding PL data (Fig. 5(a) bottom)) shows doublet states for both A- and B-excitons (indicated by red dotted lines for A-exciton and blue dotted lines for B-exciton) in reflectance spectra. The doublet spectral features related to the B-exciton state are particularly clear in the π-polarized reflectance data. This behavior is very similar to the results from bulk CdS with a subsidiary reflectivity spike found around the exciton states in the reflectance spectra, which was explained by the theory of surface repulsive potential with spatial dispersion of excitons [42]. But this feature was observed to exist only until 4.2 K [42], while in our experiments the features are visible even at 77 K. We ascribe this phenomenon to the large surface-to-volume ratio of NWs in comparison to bulk samples. The surface repulsive potential generated by the reconstruction of the surface would play an important role in the optical properties of the nanowire [21]. The detailed discussion is beyond the scope of this paper and further experiments are needed to clarify its underlying mechanism.

After careful measurements with the NW on SiO_2 substrate, the same nanowire is then transferred to the PDMS substrate by using the transfer-printing technique; the reflectance and the corresponding PL were then obtained at 77 K (Fig. 5(b)). It is clear that the exciton features including A- (~2.587 eV), B- (~2.572 eV) and C-exciton (~2.637 eV), shifted to the shorter wavelength (blue shift) compared to the results on a Si wafer. This is because the PDMS has a high thermal expansion coefficient (~310 ppm/K) [43], which is much larger than CdS (~4.6 ppm/K at 300 K to ~ -1.5 ppm/K at 80 K) [44] and therefore the blueshift can be explained by the compressive strain that the NW would experience from the shrinking of PDMS. Interestingly, the polarized reflectance spectra show that the A-exciton blue shifts significantly and crosses over the B-exciton to appear at the higher energy side. This suggests that the A-exciton is more sensitive to compressive strain than the B-exciton. To confirm this, we performed reflectance and PL measurements on a single NW both on Si substrate and on PDMS as a function of temperature (Fig. 5(c) and (d)). The temperature-dependent reflectance spectra and corresponding PL spectra are also shown in Fig. S-3. Increasing the temperature is accompanied with the releasing of compressive strain in the CdS NW (due to expansion of the PDMS substrate), and both effects will cause the energy redshift of the A- and B-excitons. By accounting for the energy shifts of A- and B-exciton on PDMS and the results on Si substrate, we can get the A- and B-exciton shift behavior predominantly induced by the compressive strain. It is evident that A-exciton and B-excitons move closer to each other with the release of compressive strain (qualitative trends shown in Fig. 5 (d)), and is consistent with the results on bulk CdS material [45]. With polarized μ-R and μ-PL measurements, strain driven A- and B-exciton energy shifts were comprehensively studied. For A-excitons, both the blue shift under compressive strain and red shift under tensile strain are very sensitive to the strain condition, while the B-excitons are not too

sensitive. The B-exciton thus becomes the lowest state in the ordering of excitons at the compressive part of the wavy NW. Thus, the PL intensity of B-excitons will dominate the PL spectra just as shown in Fig. 5(b) (bottom), and it is reasonable to assign the π-polarized Peak 1 to B-exciton emission.

To summarize, by utilizing a relatively easy approach to fabricate highly strained CdS NWs, periodic bandgap modulation along the wavy NW is demonstrated with observed shifts as large as 250 meV. By performing polarized μ-PL and μ-R measurements on single NWs, the shift behavior of A- and B-exciton as a function of strain has been characterized. Our works provides direct insights into the effect of large strains on the optical properties of NWs, which can be useful for designing mechanically responsive nanoelectronic or photonic systems. Further analysis using time-resolved measurements would shed more detailed insights about the carrier dynamics along with direct correlation with the structure of strained regions.

Supplementary Material

Refer to Web version on PubMed Central for supplementary material.

Acknowledgments

This work was supported by the U.S. Army Research Office under Grants No. W911NF-09-1-0477 and W911NF-11-1-0024, and the National Institutes of Health through the NIH Director's New Innovator Award Program, 1-DP2-7251-01. L. X. S.acknowledges travel funds from the National Natural Science Foundation of China (Grant No: 11104302).

References

1. Tombler TW, Zhou C, Alexseyev L, Kong J, Dai H, Liu L, Jayanthi CS, Tang M, Wu SY. Nature. 2000; 405:769. [PubMed: 10866192]
2. Ieong M, Doris B, Kedzierski J, Rim K, Yang M. Science. 2004; 306:2057–2060. [PubMed: 15604400]
3. Roberts MM, Klein LJ, Savage DE, Slinker KA, Friesen M, Celler G, Eriksson MA, Larally MG. Nature Mater. 2006; 5:388–393. [PubMed: 16604081]
4. Sun X, Liu J, Kimerling LC, Michel J. Appl Phys Lett. 2009; 95:011911.
5. Huo Y, Lin H, Chen R, Makarova M, Rong Y, Li M, Kamins T, Vuckovic J, Harris JS. Appl Phys Lett. 2011; 98:011111.
6. Sánchez-Pérez JR, Boztug C, Chen F, Sudradjat FF, Paskiewicz DM, Jacobson RB, Lagally MG, Paiella R. Proc Natl Acad Sci USA. 2011; 108:18893–18898. [PubMed: 22084063]
7. Smith AM, Mohs AM, Nie S. Nature Nanotechnol. 2009; 4:56–63. [PubMed: 19119284]
8. Huang M, Wu Y, Chandra B, Yan H, Shan Y, Heinz TF, Hone J. Phys Rev Lett. 2008; 100:136803. [PubMed: 18517983]
9. Hong K-H, Kim J, Lee S-H, Shin JK. Nano Lett. 2008; 8:1335–1340. [PubMed: 18402477]
10. Wu Z, Neaton JB, Grossman JC. Nano Lett. 2009; 9:2418–2422. [PubMed: 19462970]
11. Lugstein A, Steinmair M, Steiger A, Kosina H, Bertagnolli E. Nano Lett. 2010; 10:3204–3208. [PubMed: 20698638]
12. Niquet Y-M, Delerue C, Krzeminski C. Nano Lett. 2012; 12:3545–3550. [PubMed: 22694664]
13. Shiri D, Verma A, Selvakumar CR, Anantram MP. Sci Rep. 2012; 2:461. [PubMed: 22708056]
14. Greil J, Lugstein A, Zeiner C, Strasser G, Bertagnolli E. Nano Lett. 2012; 12:6230–6234. [PubMed: 23146072]
15. Wang ZL, Song J. Science. 2006; 312:242. [PubMed: 16614215]

16. Qin Y, Wang X, Wang ZL. Nature. 2008; 451:809–813. [PubMed: 18273015]
17. Wang ZL. Mater Sci and Engi Reports. 2009; R64:33–71.
18. Wang ZL. Adv Mater. 2012; 24:4632–4646. [PubMed: 22331639]
19. Han X, Kou L, Lang X, Xia J, Wang N, Qin R, Lu J, Xu J, Liao Z, Zhang X, Shan X, Song X, Gao J, Guo W, Yu D. Adv Mater. 2009; 21:4937–4941. [PubMed: 25376615]
20. Liao Z-M, Wu H-C, Fu Q, Fu X, Zhu X, Xu J, Shvets IV, Zhang Z, Guo W, Leprince-Wang Y, Zhao Q, Wu X, Yu DP. Sci Rep. 2012; 2:452. [PubMed: 22693654]
21. Wei B, Zheng K, Ji Y, Zhang Y, Zhang Z, Han X. Nano Lett. 2012; 12:4595–4599. [PubMed: 22889268]
22. Signorello G, Karg S, Björk MT, Gotsmann B, Riel H. Nano Lett. 2013; 13:917–924. [PubMed: 23237482]
23. Rogers JA, Bao Z, Baldwin K, Dodabalapur A, Crone B, Raju VR, Kuck V, Katz H, Amundson K, Ewing J, Drzaic P. Proc Natl Acad Sci USA. 2001; 98:4835–4840. [PubMed: 11320233]
24. Sheraw CD, Zhou L, Huang JR, Gundlach DJ, Jackson TN. Appl Phys Lett. 2002; 80:1088–1090.
25. Sekitani T, Kato Y, Iba S, Shinaoka H, Someya T. Appl Phys Lett. 2005; 86:073511.
26. Someya T, Sekitani T, Iba S, Kato Y, Kawaguchi H, Sakurai T. Proc Natl Acad Sci USA. 2004; 101:9966–9970. [PubMed: 15226508]
27. Khang D-Y, Jiang H, Huang Y, Rogers JA. Science. 2006; 311:208–211. [PubMed: 16357225]
28. Sun Y, Choi WM, Jiang H, Huang YY, Rogers JA. Nature Nanotechnol. 2006; 1:201–207. [PubMed: 18654187]
29. Ryu SY, Xiao J, Park W II, Son KS, Huang YY, Paik U, Rogers JA. Nano Lett. 2009; 9:3214–3219. [PubMed: 19670847]
30. Qi Y, Kim J, Nguyen TD, Lisko B, Purohit PK, McAlpine MC. Nano Lett. 2011; 11:1331–1336. [PubMed: 21322604]
31. Xu F, Lu W, Zhu Y. ACS Nano. 2011; 5:672–678. [PubMed: 21189041]
32. van Vugt LK, Piccione B, Cho C-H, Nukala P, Agarwal R. Proc Natl Acad Sci USA. 2011; 108:10050–10055. [PubMed: 21628582]
33. Agarwal R, Barrelet CJ, Lieber CM. Nano Lett. 2005; 5:917–920. [PubMed: 15884894]
34. Oulton RF, Sorger VJ, Zentgraf T, Ma R-M, Gladden C, Dai L, Bartal G, Zhang X. Nature. 2009; 461:629–632. [PubMed: 19718019]
35. Dai G, Wan Q, Zhou C, Yan M, Zhang Q, Zou B. Chem Phys Lett. 2010; 497:85–88.
36. Piccione B, Cho C-H, van Vugt LK, Agarwal R. Nature Nanotechnol. 2012; 7:640–645. [PubMed: 22941404]
37. Oulton RF, Sorger VJ, Zentgraf T, Ma R-M, Gladden C, Dai L, Bartal G, Zhang X. Nature. 2009; 461:629–632. [PubMed: 19718019]
38. Gao P, Liu K, Liu L, Wang Z, Liao Z, Xu Z, Wang W, Bai X, Wang E, Li Y. J Electron Microsc. 2010; 59:285.
39. Fu Q, Zhang ZY, Kou L, Wu P, Han X, Zhu X, Gao J, Xu J, Zhao Q, Guo W, Yu DP. Nano Res. 2011; 4:308–314.
40. van Vugt LK, Piccione B, Cho C-H, Aspetti C, Wirshba AD, Agarwal R. J Phys Chem A. 2011; 115:3872–3833.
41. Thomas DG, Hopfield JJ. Phys Rev. 1959; 116:573–582.
42. Hopfield JJ, Thomas DG. Phys Rev. 1963; 132:563–572.
43. Kunnavakkam MV, Houlihan FM, Schlax M, Liddle JA, Kolodner P, Nalamasu O, Rogers JA. Appl Phys Lett. 2002; 82:1152–1154.
44. Oskot-skill VS, Kobyakov IB, SOlodukhin AV. Fiz Tverd, Tela. 1980; 22:1479.engl : Sov Phys Solid State. 1980; 22:861.
45. Rowe, JE.; Cardona, M.; Pollack, FH. II-VI Semiconducting Compounds. Thomas, DG., editor. New York: Benjamin; 1967. p. 112

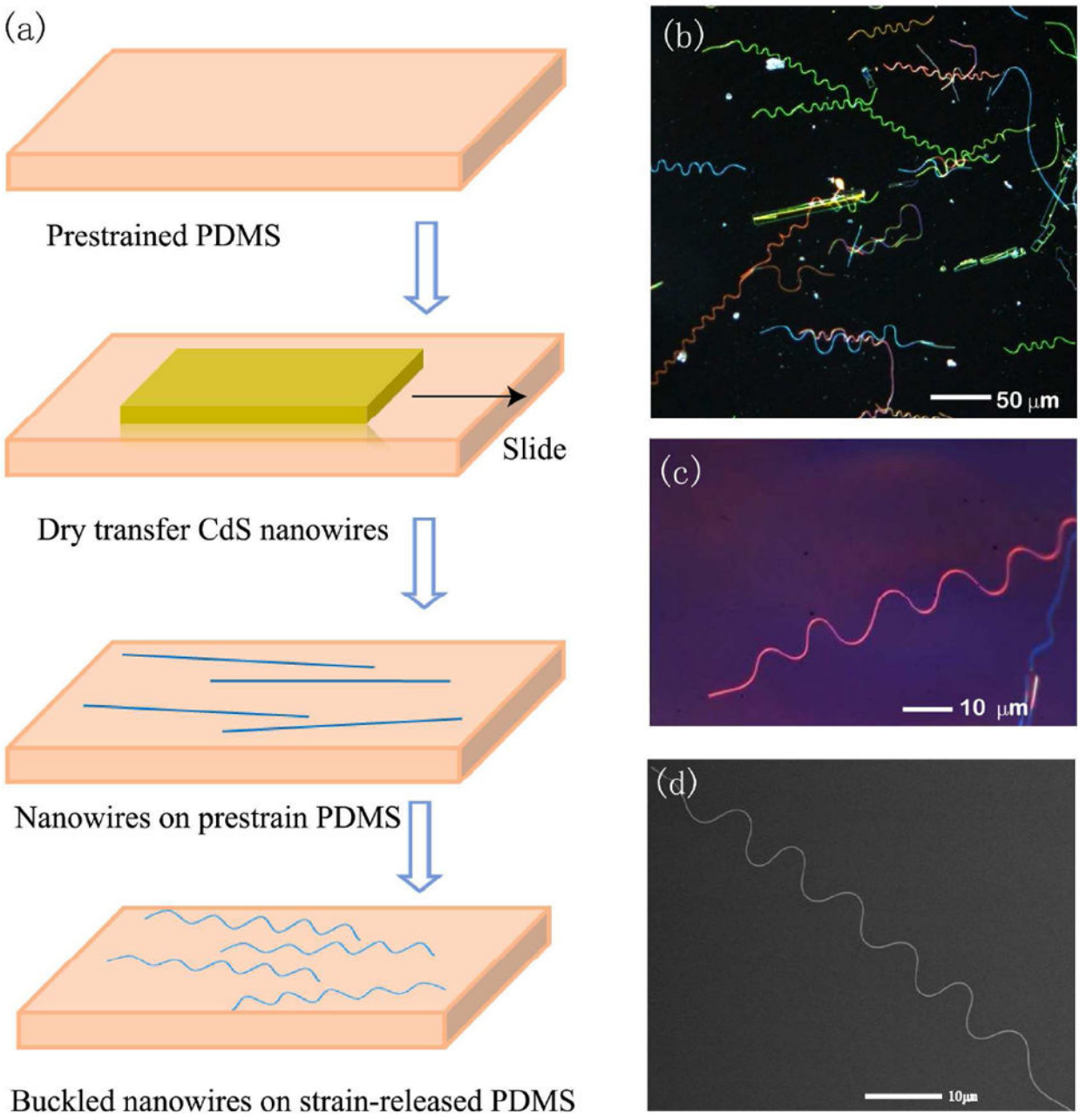

Figure 1.

(a) Schematic illustration of the process of forming buckled CdS NWs on PDMS substrates (b) Large area optical image of buckled NWs. (c) Zoomed in optical image of a single buckled CdS NW. (d) Scanning electron microscopy image of a single buckled CdS NW.

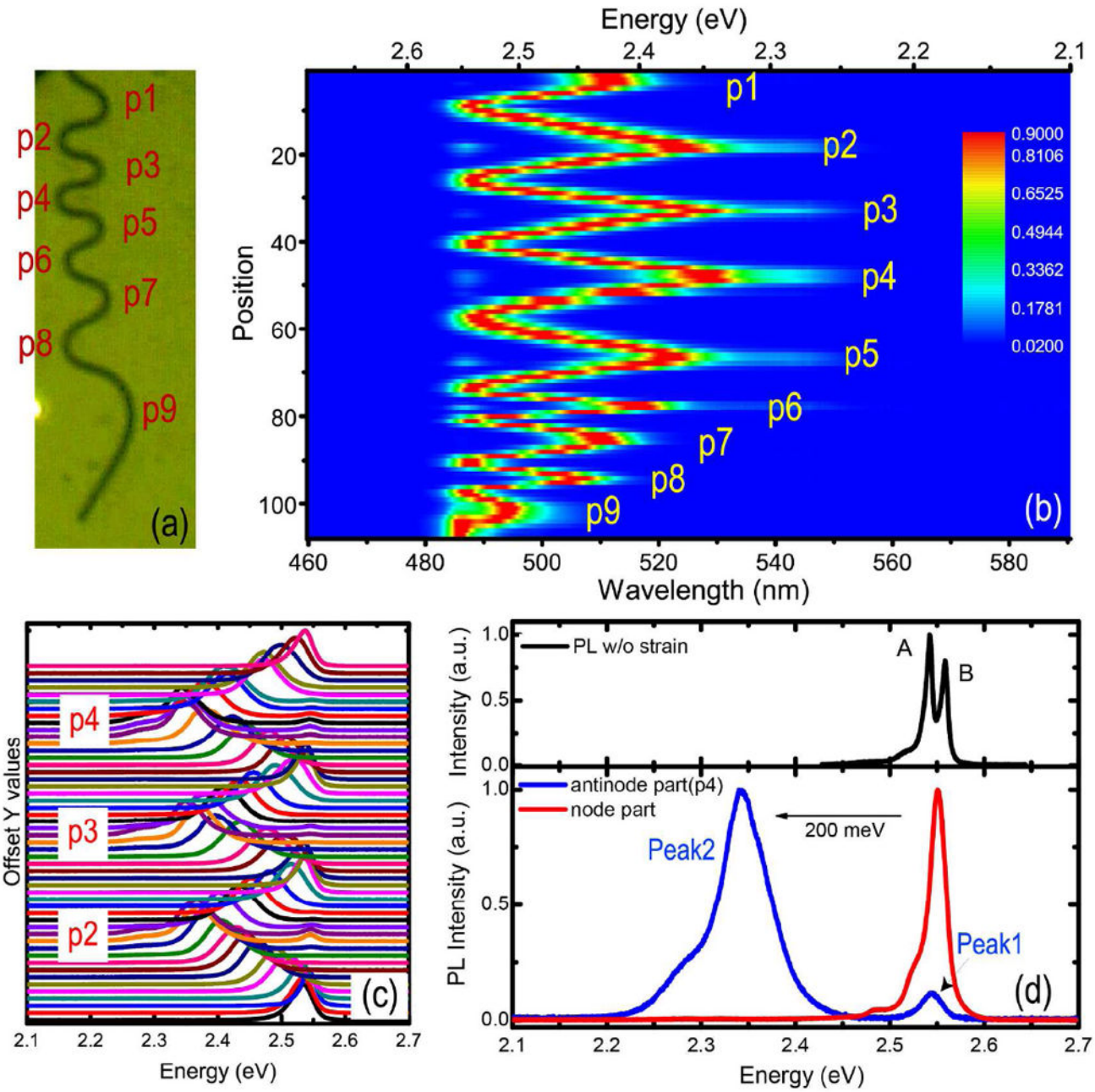

Figure 2.

(a) The optical image of a single buckled CdS NW with a wavy geometry. The antinodes regions (highly strained) of the NW are marked by labels (p1 - p9). (b) Spatially-resolved PL data of the buckled NW. Labels (p1-p9) correspond to the antinode parts in (a) at 77 K. (c) The corresponding waterfall plots of the PL spectra. (d) Spectra measured at both the node and antinode (p4) regions, and a redshift of 200 meV of the emission peak is observed (bottom). A reference PL spectrum obtained at 77K of a CdS NW on Si/SiO2 substrate (without strain) is shown (top).

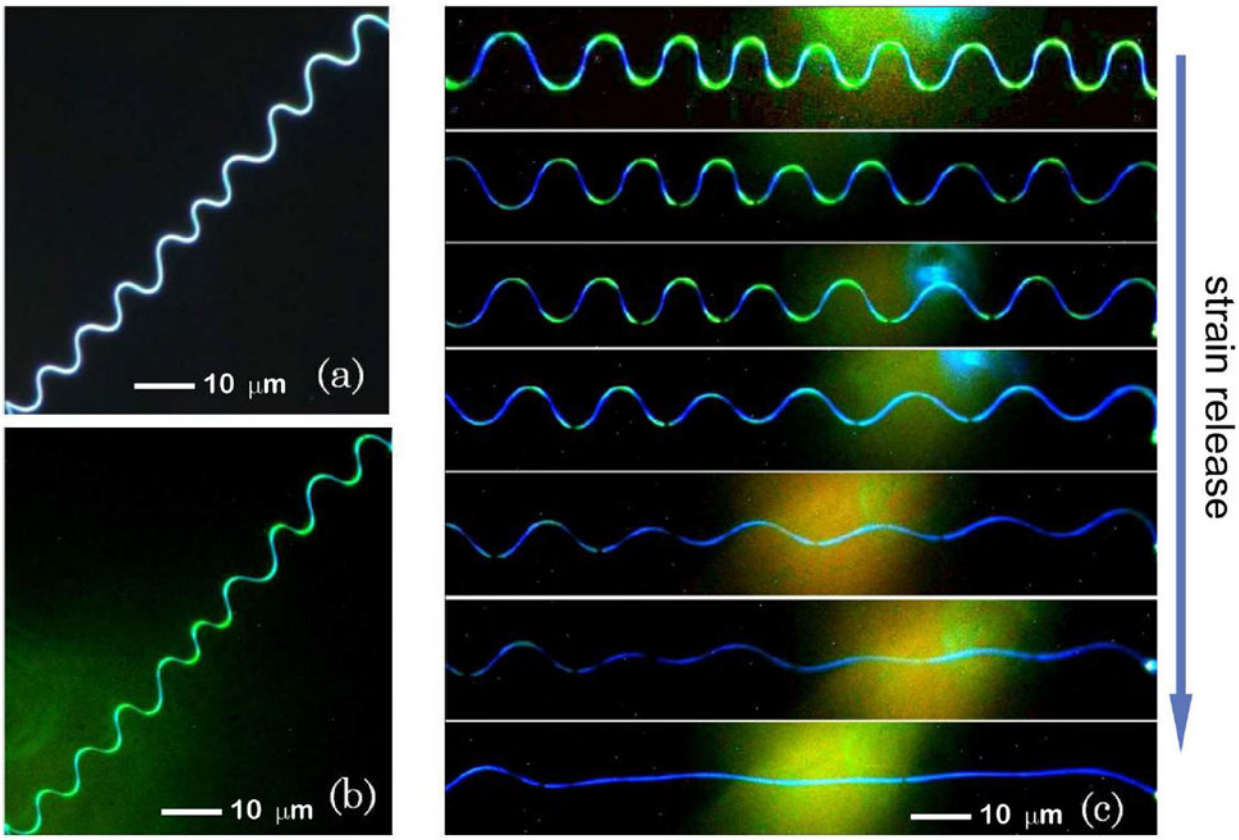

Figure 3.

(a) Dark-field optical image of a single buckled CdS NW. (b) A corresponding real-color emission image of the buckled NW obtained with a long pass 488 nm filter at room temperature. The periodic color modulation of emission from the buckled (green) to straight regions (blue) is observed. (c) By using a strain stage, the curvature of buckled NW is gradually reduced by releasing the strain (from top to bottom. This is accompanied by the change of the color from the buckled regions from green to blue, implying that the energy bandgap shift is caused by the change in the deformation potential.

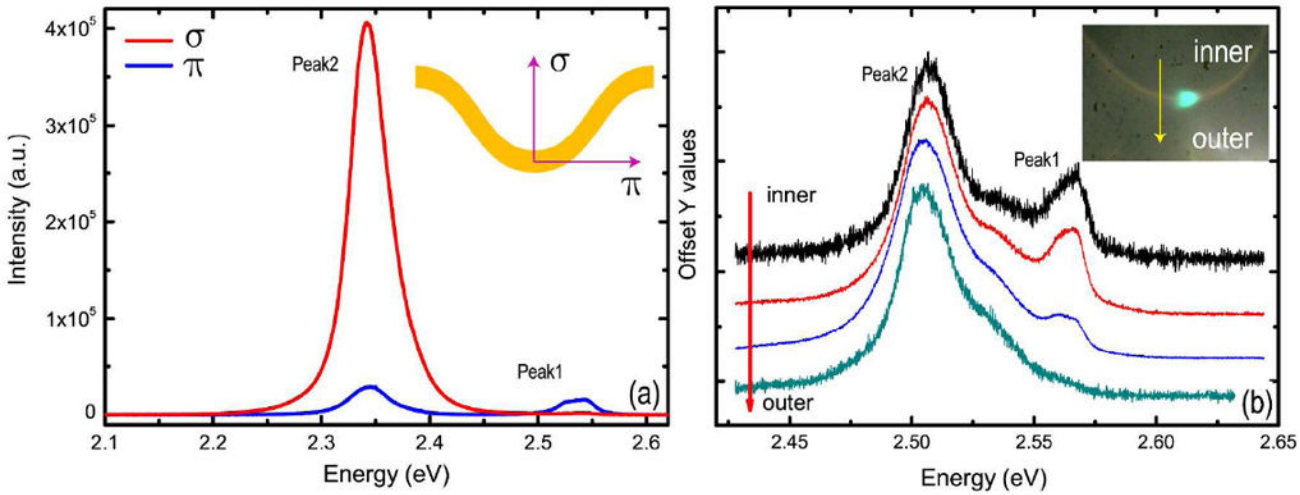

Figure 4.

(a) Polarized PL spectra from the antinode region of a wavy CdS NW at 77 K. Inset schematically illustrates the polarization configurations, σ- and π-polarized. (b) Spatially-resolved PL spectra measured along the cross-section of the NW (diameter, 300 nm) from the inner (compressive) to the outer part (tensile) as shown in the inset. It is observed that the π-polarized Peak 1 gradually disappears as the excitation laser moves from the compressive to the tensile regions of the NW cross-section.

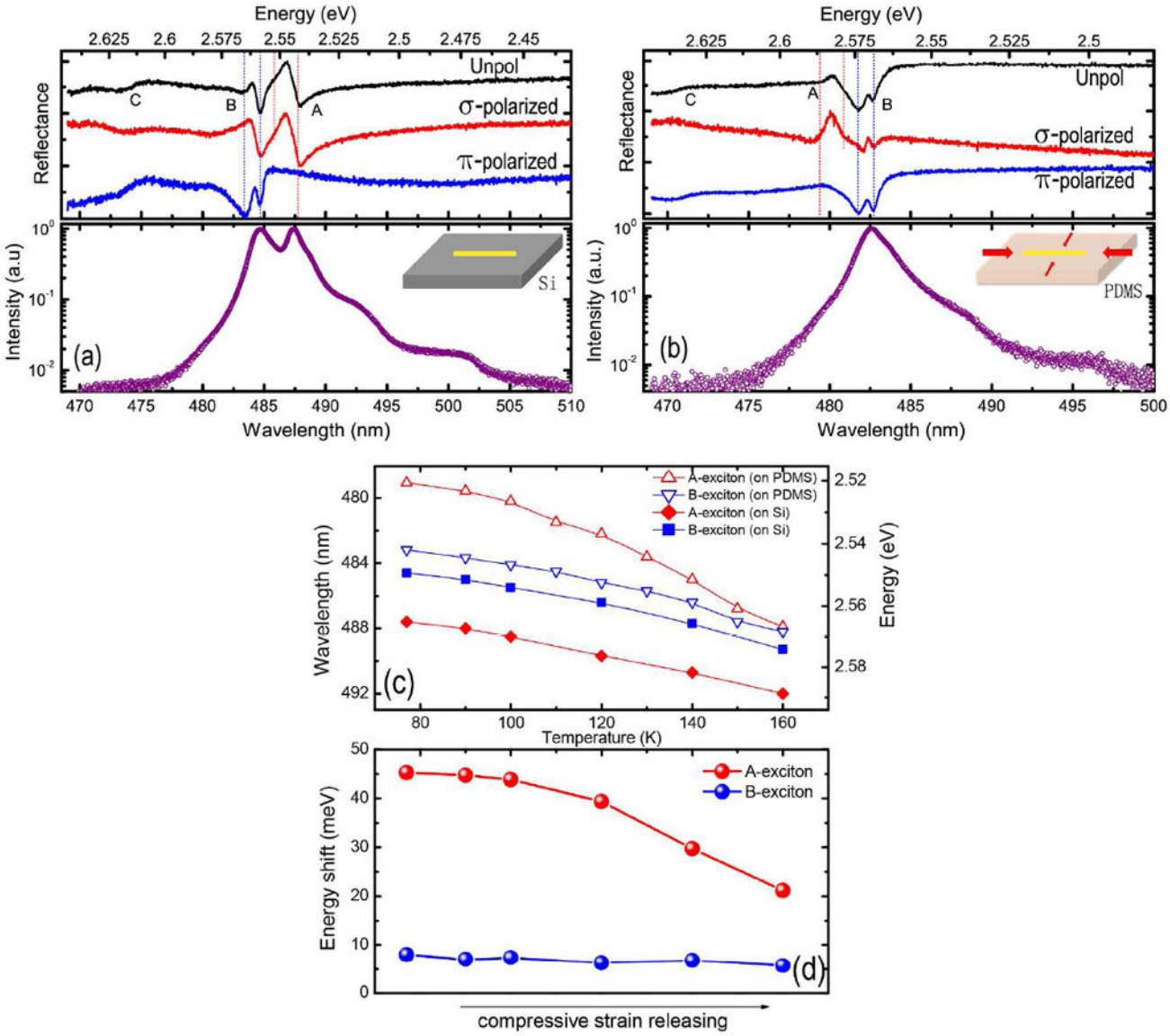

Figure 5.

(a) Polarization-resolved reflectance (top) and PL (bottom) spectra of a single CdS NW dispersed on a Si substrate (with a 300 nm SiO_2 layer) at 77 K. Features corresponding to the A-(red dotted lines), B- (blue dotted lines), and C-excitons are clearly observed from the reflectance data. (b) Polarization resolved reflectance and PL spectra of the same CdS NW transferred from Si to a PDMS substrate. Due to the low temperature induced shrinking of PDMS, the NW is strongly compressed by the PDMS substrate. A-, B-, and C-excitons show a blueshift, and the A-exciton appears to be more sensitive to strain in comparison to the B- and C-excitons. The A-exciton in fact crosses over to the B-exciton and now appears at the high energy side. (c) The A- and B-exciton shifts as a function of temperature measured with a NW both on PDMS substrate and on Si substrate, respectively. Increasing the temperature is accompanied with the release of compressive strain on the CdS NW (due to PDMS), and both effects cause the redshift of A- and B-excitons. In order to get the trend

of the exciton energy shifts solely induced by the strain, corrections are made to account for energy shifts of A- and B-exciton on PDMS and on Si substrate, the results are shown in (d).